JOURNAL OF GEOPHYSICAL RESEARCH, VOL. ???, XXXX, DOI:10.1029/,

Remote sensing of mesospheric dust layers using active modulation of PMWE by high-power radiowaves

A. Mahmoudian,[1] , A. Mohebalhojeh,[1] , M. Farahani,[1] , W. A. Scales,[2] , M. Kosch,[3,4,5]

alirezam@vt.edu

[1]Institute of Geophysics, University of Tehran, Tehran, Iran

[2]The Bradley Department of Electrical and Computer Engineering,Virginia Tech, USA

[3]South African National Space Agency, Hermanus 7200, South Africa

[4]Physics dept., Lancaster University, Lancaster LA1 4YB, UK

[5]Physics dept., University of Western Cape, Cape Town 7537, South Africa

Abstract.

This paper presents the first study of the modulation of polar mesospheric winter echoes (PMWE) by artificial radiowave heating using computational modeling and experimental observation in different radar frequency bands. The temporal behavior of PMWE response to HF pump heating can be employed to diagnose the charged dust layer associated with Mesospheric Smoke Paricles (MSP). Specifically, the rise and fall time of radar echo strength as well as relaxation and recovery time after heater turn-on and off are distinct parameters that are a function of radar frequency. The variation of PMWE strength with PMWE source region parameters such as electron-neutral collision frequency, photodetachment current, electron temperature enhancement ratio, dust density and radius is considered. The comparison of recent PMWE measurements at 56 MHz and 224 MHz with computational results is discussed and dust parameters in the PMWE generation regime are estimated. Predictions for HF PMWE modification and its connection to the dust charging process by free electrons is investigated. The possibility for remote sensing of dust and plasma parameters in artificially modified PMWE regions using simultaneous measurements in multiple frequency bands are discussed.

1. Introduction

So-called polar mesospheric winter echoes (PMWE) are radar echoes observed during the polar winter at altitudes around 50–80 km and are much weaker than their PMSE (Polar Mesospheric Summer Echoes, e.g. Rapp and Lubken, 2004) counterpart and also much less studied. Breaking of gravity waves and the associated turbulence are proposed as the major source for PMWE echoes. The action of neutral turbulence alone does not appear to give a good explanation for PMWE. The close similarity in spectral widths inside and outside the PMWE source region lends evidence to this assertion (Kirkwood et al., 2006a, 2006b; Zeller et al., 2006). It should be noted that so-called PMSE are due to Bragg scatter from electron irregularities which result from charging of free electrons and ions onto subvisible ice particles (e.g. Inhester et al., 1994). While some theories can explain the PMWE characteristics only by the turbulence, there are rocket and radar observations that show the presence of nanometer scale particles throughout PMWE regions (Baumann et al., 2013). Ablation and evaporation of meteors in the atmosphere between 60 km and 90 km are the main source of Mesospheric Smoke Paricles (MSP). These particles may influence electron density fluctuations through charging and as a result radar echoes (Lubken et al., 2006). MSPs therefore have been proposed to exist in the PMWE source region and lead to electron irregularities that produce the radar echoes (Havnes and Kassa, 2009). Most previous PMWE observations were during enhanced electron density conditions. Charging of MSP by free electrons (Friedrich et al., 2012) and ion chemical reactions (Kero et al., 2008) are the two main sources of electron reduction in PMWE region. There have been recent studies of the seasonal and monthly variation of PMWE in

the austral hemisphere observed by the PANSY (Program of the Antarctic Syowa MST/IS) radar in 2013 (Nishiyama et al., 2015). According to these observations, ionization during energetic electron precipitation was the possible cause of PMWE and the strongest PMWE was reported in May. A review of continuous observations of PMWE at northern latitudes using the ALWIN VHF radar located at the Norwegian island Andoya (69.30N, 16.04E) (2004–2008) and the Middle Atmosphere Alomar Radar System (MAARSY) (since 2011) has been reported by Latteck and Strelnikova (2015). Based on these observations, the PMWE occurrence depends on the time of the day (or solar zenith angle) which indicates the strong dependence on electron density. It has been shown that September is the beginning of PMWE appearance (Latteck and Strelnikova, 2015). It should be noted that MSP responsible for PMWE and ice particles associated with PMSE are referred to as dust throughout this paper for simplicity of notation.

The impact of heating the PMSE source region with high power radiowaves has been studied extensively using computational models as well as experimentally at EISCAT with 7.9 MHz, 56 MHz, 224 MHz, and 930 MHz after the first observations of Chilson (2000) showed suppression of PMSE after heater turn-on. Pumping the plasma with radio-waves enhances the electron temperature which affects diffusion and charging of any ice particle present. The temporary enhancement of PMSE after heater turn-off, described as the PMSE overshoot, was observed in experiments by Havnes et al. (2003) and Havnes (2004). The first theoretical model was developed by Havnes (2004) to explain the overshoot effect after heater turn-off for VHF radar data. Enhancement of HF PMSE after heater turn-on was predicted by Chen and Scales (2005). Mahmoudian et al. (2011) made the first detailed calculations of the effect of different plasma and dust (ice particle)

parameters on PMSE turn-on overshoot. The dust parameters (density and radius) for turn-on overshoot at 56 MHz and 7.9 MHz were predicted. The first modulation of high-frequency (HF, 7.9 MHz) PMSE at EISCAT was observed by Senior et al. (2014). This behavior was interpreted as a result of dominant dust charging over plasma diffusion which is in line with the model predictions. The ice particle radii and concentration were estimated using the comparision of HF and VHF PMSE with the computational model (Senior et al., 2014). Havnes et al. (2015) also reported the comparison of observations of modulated PMSE at 224 MHz and 56 MHz with model predictions. Although there was in alignment with model predictions, it was suggested that the discrepancies between the observations and model were due to limitations in physical processes incorporated in the charging model. It should be noted that Biebricher et al. (2012) developed a computational model that is in line with these experimental observations as well.

The first active modulation of PMWE observed by the 224 MHz radar was conducted by Kavanagh et al., (2006). A 10 s heating cycle was used during this experiment and a suppression of PMWE by a factor of 93% was observed. This experiment was repeated by Belova et al., (2008) with a 20s on and 160 s off heating cycle. A 50% reduction of signal strength during heating turn-on and a turn off overshoot was reported. La Hoz and Havnes (2008) reported a similar observation at 56 MHz with 70 percent reduction of the radar signal during heating. Havnes et al. (2011) repeated the experiment which shows a small recovery of signal intensity during HF-pump on period and an enhancement of $\sim$15% after heater turn-off were observed. Both effects are attributed to charging of free electrons onto the dust particles as a result of enhanced background electron temperature due to HF pumping. Another PMWE heating measurement using EISCAT VHF radar

(224 MHz) was reported by Kero et al., (2008). The electron temperature was estimated to be around 5 times the neutral temperature during heater turn-on. The comparison between the electron density variation during heater on and off period using Sodankyla Ion chemistry model (SIC) and the observations has shown the signature of negative charged particles (Kero et al., 2008). Therefore, active modulation of PMWE mainly depends on the presence of MSPs in the vicinity of PMWE source region (50-80 km) which is due to the modified charging process of free electrons on to MSP through electron temperature enhancement.

The only study on modeling of PMWE heating experiments was done by Havnes and Kassa., (2009). The finite diffusion timescale was overlooked by treating electrons and ions using the Boltzmann approximation. It should be noted that the Havnes model was limited to high radar frequencies, small dust sizes and low dust densities because of incorporating the Boltzmann approximation and neglecting finite diffusion time effects. The computational model developed by Chen and Scales (2005) and Mahmoudian et al. (2011) is able to simulate the time evolution of HF modulated PMSE in all radar frequency bands. This model is incorporated in this paper. The objective of this paper is to consider the temporal variation of PMWE during heating on and off cycles to obtain diagnostic information about the source region. Radar frequencies used in this paper are based on the available facilities at EISCAT and HAARP (The High Frequency Active Auroral Research Program). The importance of charging and diffusion timescales in the PMWE source region is first discussed. Key differences in the PMWE and PMSE parameter regimes are emphasized. According to recent in-situ measurements using rocket payloads (e.g. Robertson et al., 2009), there is significant uncertainty as to the charging

process of dust particles in space which are not consistent with the standard charging theory. Therefore, a modified charging model including photoemission current and positive dust particles is adopted in this work. A comparison of the data collected during VHF PMWE modulation experiments using 56 MHz and 224 MHz with computational results is presented. The possible diagnostic information for charged dust and background plasma parameters is discussed. Predictions on the temporal evolution of HF PMWE modulation and its implications on characterizing the dust charging process are considered in section 4. Finally, a summary and conclusion is provided.

2. Modeling

2.1. Computational model

The computational model previously used to study the active modification of PMSE is adopted to study the PMWE heating. The model used in this study is a hybrid model including fluid plasma and particle in cell (PIC) dust (Scales, 2004; Chen and Scales, 2005; Mahmoudian et al., 2011). A continuous charging model based on the Orbital-Motion-Limited (OML) approach has been used for the time varying charge on the dust particles. Unlike the previous models developed by Havnes and Kassa (2009), the model presented here enables the study of the evolution of electron irregularity amplitude at a range of relevant frequency, plasma and dust parameters. Variation of the ion density (the electron density n_e is determined by quasi-neutrality) is described by the continuity equation:

$$\frac{\partial n_{\mathrm{i}}}{\partial t} + \frac{\partial}{\partial x}(n_{\mathrm{i}} v_{\mathrm{i}}) = P_{\mathrm{i}} + L_{\mathrm{i}} + \frac{\mathrm{d}n_{\mathrm{i}}}{\mathrm{dt}}|_{\mathrm{charging}}, \tag{1}$$

where $L_{\rm i}$ denotes the loss due to dissociative recombination and $P_{\rm i}$ denotes the ion production due to photoionization and energetic particle precipitation. The last term in Eq. (1) represents the ion reduction due to charging onto the dust particles. The recombination rate is modeled using $L_{\rm i} = \gamma n_e n_i$ with a recombination rate coefficient γ. Neglecting inertial effects in the momentum equation, the ion velocity can be written in this form,

$$v_{\rm i} = \frac{1}{\nu_{\rm in}} \left(\frac{q_{\rm i}}{m_{\rm i}} E - \frac{K T_{\rm i}}{m_{\rm i}} \frac{\partial}{\partial x} (\log(n_{\rm i})) \right), \tag{2}$$

where q_i, m_i,T_i and ν_{in} are the ion charge, mass, temperature and ion-neutral collision frequency, respectively. The electrostatic field (E) is determined using a current closure condition in ionospheric plasma and to a good approximation is (Mahmoudian et a., 2011)

$$E \approx -\frac{K T_e}{e} \frac{\partial}{\partial x} (\log(n_{\rm e})) \tag{3}$$

The winter polar mesopause temperature for both ions and electrons is taken to be $T_e = T_i = 250$ K. The ion-neutral collision frequency is of order 5×10^5 s^{-1}. The electron-neutral collision frequency temperature dependence is assumed to be $\nu_{en} \propto T_e$ and recombination rate dependence on temperature is taken to be $\gamma \propto T_e^{-1/2}$. The electron density is assumed to be 10^8 m^{-3}. Recent rocket measurement has detected meteoric smoke particles in the D-region (altitude range 65-75 km) with 1 nm $< r_d <$ 5 nm and $n_d = 10^9$ m^{-3} (Baumann et al., 2013). Larger MSPs 5 nm $< r_d <$ 15 nm with $n_d = 10^8$ m^{-3} were also observed by Baumann et al., (2013). Hunten et al., (1980) predicted large MSP densities below 1 nm. Although due to limitations on the most of rocket experiment dust particles smaller than 1 nm were not detected (Baumann et al., 2013), however, recent in-situ measurements have

revealed the tiny MSP with radii of less than 1 nm (e.g., Strelnikova et al., 2007; Fentzke et al., 2009; Robertson et al., 2014). Due to the limitations of the model presented for dust particles smaller than 1 nm and especially at lower radar frequencies, a minimum dust radius of 1 nm will be used throughout this work as part of the model constraints. Although considering dust radius distribution from 0.5 nm to 1.5 nm is expected to not change the results much. Collision frequencies are higher in the PMWE region by a factor of 5 to 10 in comparision with the PMSE region (Schmitter, 2011).

The charging model used in this study has been modified with respect to the model used in the previous study by including the photodetachment current (Mahmoudian et al., 2011). The time variation of charge on dust particles based on continuous Orbital-Motion-Limited OML approach (Bernstein and Rabinowitz, 1959) can be written as follows:

$$\frac{dQ_d}{dt} = I_e + I_i + I_P \tag{4}$$

where I_e, I_i, and I_P are the electron and ion current on each dust particle, and photo-detachment current, respectively. The currents on to the negatively charged dust particles are given by:

$$I^{\mathrm{OML}}_{\mathrm{e,Z_d<0}} = \sqrt{8\pi} r_d^2 q_e n_e v_{te} \exp(-\mathrm{q_e}\phi_\mathrm{d}/\mathrm{KT_e}) \tag{5}$$

$$I^{\mathrm{OML}}_{\mathrm{i,Z_d<0}} = \sqrt{8\pi} r_d^2 q_i n_i v_{ti} (1 - q_i\phi_d/KT_i) \tag{6}$$

For positive dust particles ($Z_d > 0$), the ion and electron currents are given by:

$$I^{\mathrm{OML}}_{\mathrm{e,Z_d>0}} = \sqrt{8\pi} r_{\mathrm{d}}^2 q_{\mathrm{e}} n_{\mathrm{e}} v_{\mathrm{te}} (1 - q_{\mathrm{e}}\phi_{\mathrm{d}}/KT_{\mathrm{i}}), \tag{7}$$

$$I^{\mathrm{OML}}_{\mathrm{i,Z_d>0}} = \sqrt{8\pi} r_{\mathrm{d}}^2 q_{\mathrm{i}} n_{\mathrm{i}} v_{\mathrm{ti}} \exp(-q_{\mathrm{i}}\phi_{\mathrm{d}}/KT_{\mathrm{e}}). \tag{8}$$

Here, r_d is the dust radius, $n_{e(i)}$ electron (ion) density, $T_{e(i)}$ electron (ion) temperature, K Boltzmann constant, $q_{e(i)}$ electron (ion) charge, Z_d dust charge, $v_{te}(i)$ electron (ion) thermal velocity and ϕ_{d} dust floating potential. Assuming negative charged dust, photo-detachment current can be approximated by (Rosenberg, 1996)

$$I_{\mathrm{P,Z_d<0}} = -\pi r_d^2 \alpha, \tag{9}$$

For positive grains, it can be shown that an approximation is

$$I_{\mathrm{P,Z_d>0}} = -\pi r_d^2 \alpha \exp(\mathrm{q_e}\phi_{\mathrm{d}}/\mathrm{KT_p}), \tag{10}$$

where r_d is the dust radius. In Eq.(9) and (10), the parameter α is $\alpha = q_e J_p Q_{ab} Y_p$ where q_e, J_p, Q_{ab}, Y_p, and T_p are the electron charge, photon flux, photon absorption efficiency, photoelectron yield, and average photoelectron temperature. Previous study has estimated solar photon flux J_p of the order of $\sim 1.5\times10^5$ photon cm^{-2} s^{-1} for $h\nu$ $\sim$4-5 eV and the absorption efficiency $Q_{ab} \sim 1$ (e.g. Brasseur and Simon, 1981). Photoelectron yield Y_p can also be estimated using $Y_p = C(h\nu - W)^2$, with $C = 0.01/(eV)^2$ (Rapp and Lubken, 1999). Q_{ab} is assumed to be $\sim$1 for $2\pi r_d/\lambda > 1$, where λ is the wavelength of the incident photons (Shukla and Mamun, 2002). Calculations by Rapp (2009) indicate that

photo-detachment current is important for sufficiently small radii (1 nm) and metallic compounds (e.g. Fe_2O_3 , SiO). The average photoelectron temperature T_p is assumed to be $\sim 400 T_e$. The previous studies have shown that MSP present in the mesosphere may be positively charged due to photoemission by solar UV radiation (Rosenberg and Shukla, 2002). Rosenberg et al., (1996) provided an estimation of photo-emission current for UV intensity of 8-9 eV photon.

2.2. Physical Time-scales

The temporal behavior of the PMWE radar signal after heater turn-on depends on two physical processes. The diffusion process tends to suppress the electron density fluctuation amplitude. On the other hand, the charging process of free electrons onto the dust particles tends to enhance the density fluctuation amplitude. Depending on which process occurs in a shorter timescale, the corresponding radar echoes may increase or decrease after the heater turn-on. The timescale for electron attachment onto the dust at the initial time after turn-on of the radio wave is approximated by:

$$\tau_{chg} \approx \frac{e}{I_e} = \frac{1}{\sqrt{8\pi} n_{e0} v_{te} r_d^2 (1 - q_{\mathrm{e}} \phi_{\mathrm{d}} / K T_{\mathrm{e}})} \tag{11}$$

where v_{te}, n_{e0}, and ϕ_{d} are electron thermal velocity, electron density, and dust floating potential (Mahmoudian et al., 2011). T_{e} denotes electron temperature and r_d is the dust radius. As can be seen, electron charging time scale depends on T_e and is expected to be reduced as the T_e/T_i increases during heating. The diffusion timescale can be approximated by (Chen and Scales, 2005):

$$\tau_{\rm diff} \approx \nu_{in}(\frac{\lambda_{irreg}}{2\pi v_{\rm ti}})^2 \frac{1}{(1+\frac{T_e}{T_i}(1+\frac{z_{d0}n_{d0}}{n_{e0}}))} \quad (12)$$

where ν_{in} is the ion-neutral collision frequency, λ_{irreg} is the irregularity wavelength and v_{thi} is ion thermal velocity. z_{d0}, n_{d0}, and n_{e0} are dust charge, dust density, and electron density. According to the Bragg scattering condition $\lambda = 2\lambda_{irreg}$ where λ is the radar wavelength. The diffusion timescale is a function of scale-size of electron density fluctuations. Therefore, for larger irregularity wavelengths (or lower radar frequencies), the charging timescale may be smaller than the diffusion timescale. The electron density fluctuation amplitude and radar backscattered signal in the HF band are expected to be enhanced after the heater turn-on. The diffusion timescale for typical winter mesospheric parameters (section 2.1) is of the order of $\sim$ 200 sec, $\sim$ 4 sec, and $\sim$ 0.2 sec for frequencies 8 MHz, 56 MHz, and 224 MHz, respectively.

According to the computational results, including the photo-detachment current results in a lower charge state on the dust particles and, in general, extends the charging timescale. A large portion of small particles may remain neutral by including photo-detachment current compared to much larger dust particles (Havnes and Kassa, 2009). Including photo-detachment current depending on the parameters significantly impacts the charge state of small MSP. As a result, photo-detachment current leads to a weaker PMWE and suppresses the modulation of PMWE by high power radiowaves. The photo-detachment timescale can be described as $1/(\pi r_d^2 \alpha)$. Therefore, increasing the value of α reduces the photo-emission timescale which can dominate the charging and diffusion process. Including photo-detachment current may result in positively charged dust particles especially for small dust particles associated with PMWE region. The presence of

positive dust particles can cause substantial change in the electron irregularity amplitude (radar echoes) and will be discussed in the following paragraph.

As an example Figure 1 shows the effect of photo-detachment current on the charged dust particles associated with radar frequency 224 MHz. Dust radius r_d is assumed to be 1.5 nm, dust density n_d/n_{e0} 150%, $T_e/T_i = 2$ and $\nu_{in} = 10^5$ Hz. The photo-detachment coeffient α is varied from 0 to 1 where zero denotes no photo-detachment. Figure 1b shows the variation of electron and ion currents during HF pump heating at 224 MHz. As can be seen in Figure 1b, increasing the photo-detachment coefficient results in higher density of neutral particles as it reduces the electron current onto the dust particles. Small portion of dust particles (a few percent) will be charged positively in the case of high values of α. This is predicted in the previous study by Knappmiller et al., (2011) that showed less than 9 percent of MSP with $r_d = 1$ nm will have a positive charge in the presence of photo-detachment current. As α increases, the number of neutral and positive dust particles increases. As shown in Figure 1a, increase of positive and neutral dust particles is equivalent to the case of low dust density. The presence of positive particles and high neutral density results in a reduced charging timescale (due to high value of n_e/n_d) and a fast recovery of VHF PMWE during heater on period is expected (as shown in Figure 1 for $\alpha = 0.1$ and 0.08). The large enhancement of turn-off overshoot for high values of α, is also due to enhanced ion discharging current. Therefore, including photo-detachment process especially for small dust particles has a significant effect on the temporal evolution of radar echoes.

It should be noted that the squared electron density fluctuation amplitude $(\delta n_e/\delta n_{e0})^2$ is related to backscattered radar signal. The following expression represents the relationship between the irregularities and the radar reflectivity (Ryrvik and Smith, 1984):

$$\sigma(k) = n\frac{\pi}{8}k^2\frac{f_{pe}^4}{4f^4}\frac{Sn_e(k)}{n_e^2} \tag{13}$$

where $k = 2\pi/\lambda$ and f are the wave number and frequency of the radio wave in Hz, λ is the wavelength, $\sigma(k)$ denotes the radar scattering cross-section per unit volume, f_{pe} is the electron plasma frequency, n is the exponent of the electron power spectral density, and $Sn_e(k)$ is the 1-D power spectrum of the electron irregularities. Chen and Scales (2005) have shown that Eq. (13) can be simplified to $\sigma(k) \sim \delta n_e^2$ for the sinusoidal density perturbations considered in this study.

3. Experimental Observations

3.1. Case study I (56 MHz)

Recent PMWE heating observations by Havnes et al., (2011) using MORRO radar (56 MHz) imply the presence of dust particles in the source region. Figure 2 shows the PMWE under artificial electron heating using 56 MHz radar reported by Havnes et al., (2011). A heating cycle of 20 s on and 100 s off is used. The observations show a relaxation time of about 60-70 s. Photo-detachment which plays an important role in the charge state of small MSPs, has been proposed as the main candidate for the observed relaxation rates (Havnes et al., 2011). Ion attachment to negative dust particles and discharging were ruled out due to small size of dust particles present in PMWE.

The main goal of simulations shown in Figure 3a is to study the dusty plasma (including small MSP) parameters associated with observations shown in Figure 2 by including small dust particles in the model as well as photo-detachment current. The reason for choosing such a small particle size is to study the relaxation time after the heater turn-off and compare that with the experimental data shown in Figure 2. It should be noted that T_e/T_i was estimated to be around 3 during this experiment. The same ratio for T_e/T_i has been considered in the simulations. As can be seen in Figure 3a, the dashed line shows the simulation results for r_d =2.5 nm and solid lines denotes the results for r_d =2 nm. The photo-detachment coefficient α is assumed to be 0.001 in all cases. Higher dust densities are considered for smaller dust radius to get the best agreement with the experimental data. As can be seen in Figure 3a, all cases show a reduction of radar signal by about 80% during heating which are consistent with the observations shown in Figure 2. A sharp increase of signal amplitude right after the turn-off to its value before the heater turn-on is predicted which is of the order of 3 sec. This is in agreement with the experimental data which shows the increase of radar echo strength within 5 sec after the heater turn-off. The maximum amplitude of turn off overshoot of the order of 1.2 is predicted for r_d = 2 nm, n_d =320 % and r_d = 2.5 nm, n_d =235 %. The main difference between the cases with r_d =2 nm and 2.5 nm is the behavior of radar signal during heater turn-off and after the maximum amplitude is reached. According to Figure 3a, dust radius 2.5 nm shows a faster decay after the heater turn-off to the initial amplitude. The relaxation time after the heater turn-off is about 65 s for dust radius 2.5 nm which is in reasonable agreement with the experimental observations. The relaxation time estimated for r_d =2 nm is about 100 sec. Havnes et al., (2011) proposed the photo-detachment current as the main reason

for the observed relaxation time. Considering the computational results presented in Figure 3a, combination of photo-detachment current and small dust radius produce the best agreement with the observations. This contradicts the conclusion of Havnes et al. (2011) who overlooked the role of small dust particles on such a long relaxation time. It should be noted for ν_{in} larger than 10^5 Hz, a small turn-on overshoot is observed (within 5 s of heater turn-on) in the numerical simulations. The presence of the turn-on overshoot at 56 MHz is possible and may not be observed due to high absorption rate at 8 MHz or low time resolution of the radar.

Figure 3b shows the calculated behavior of PMWE at 56 MHz for larger dust radii (4 nm). The electron temperature enhancement ratio is assumed to be 3 and 4 to be consistent with the experimental observations by Havnes et al., (2011) which predicted $T_e/T_i \sim 3$ for the altitude range 60 to 62 km. Three sets of parameters with r_d =4 nm are used to determine the dust parameters associated with Figure 2. The main difference between the observations and computational model is the fall time or the time for the minimum amplitude of 0.2 after the heater turn-on to be reached. The observation shows a fall time less than 4 s, but Figure 3b represents a slow decay of the order of 10-15 s. This is mainly due to small particle sizes used in the simulation. The sharp decrease in the experimental data could be a result of enhanced D-region absorption. The minimum amplitude matches the observations well. The dashed line (T_e/T_i =4, n_d =60%) and solid black line (T_e/T_i =3, n_d =65%) show the turn-off overshoot amplitude of 1.2 which is consistent with observations (Figure 2). The main difference between Figures 3a and 3b is the behavior of radar signal after the heater turn-off. As can be seen in Figure 3b, the amplitude of radar echo decreases to values below 1 and then recovers to the value before

heater turn-on. Therefore, increasing the dust radius to 4 nm can not produce similar results to the observations after the heater turn-off.

Three main parameters have been considered to compare the comutational results with the observations. The mimimum amplitude of radar echoes at 56 MHz during heating, the time that the maximum turn-off overshoot is reached, and decay of radar echoes to their initial value during heater turn-off (relaxation time) are the main characteristics of radar signal considered to compare the model and the observations. As discussed above and a close comparision of Figures 3a and 3b with the observations illustrated in Figure 2 shows that smaller dust particles ($\sim$ 2 nm) produce the best agreement with the experimental data.

3.2. Case study II (224 MHz)

Belova et al., (2008) presented the overshoot effect during active modulation of PMWE detected by VHF radar (224 MHz). A sharp decrease in power within 2 s after X-mode turn-on and a sharp increase after turn-off were observed during PMWE modulation. As can be seen in Figure 4, the data recorded during this experiment show a 50 % decrease in echo strength when the heater was turned-on. The heater was on for 20 s and off for 160 s. No recovery was observed during heating that was attributed to the existence of dust particles with radii larger than 10 nm (Belova et al., 2008). The echo strength increases about 50% beyond the undisturbed level within 2 s after heater turn-off. The relaxation time of echo power to the undisturbed level is about 20 s.

The computational model described in the section 2 is used with different parameters set to obtain the best agreement with the observations. Dust radius of 1 nm, n_d = 320 % as well as r_d =1.5 nm and n_d =210% are considered. The solid curve associated with

$r_d = 1$ nm shows good agreement with the experimental data during the heater turn-off (Figure 4), but it shows an overestimate of the order of 0.2 for the turn-off overshoot. The dashed and dotted lines represent the temporal evolution of PMWE with including the photodetachment current for the same parameter sets. As can be seen in Figure 5a including photodetachment current with α =0.005 in Eq. (9) and (10), shifts the curve about 0.1 during heater on and off period which matches the experimenal observations shown in Figure 4 well. This effect could be due to the increase of neutral density and enhancement of ν_{in} which directly increase the diffusion time-scale. Therefore, less suppression of radar signal strength is expected during HF pump heating with including photo-detachment current. It is note-worthy that including photodetachment current does not change the recovery time after the initial suppression during heater turn-on. The turn-off overshoot appears in about 1 s after the heater turn-off and decay time is of the order of 20 s which are consistent with the observations.

The variation of plasma-neutral collision frequency and its effects on the time evolution of PMWE at 224 MHz is shown in Figure 5b. In-situ measurements in the altitude range 70 km to 80 km in the mesosphere have detected meteoric smoke particles (MSP) with densities around 10^8 m^{-3} and radii about 5 nm (Baumann et al., 2013). Dust radius is assumed to be 4 nm in the simulation. ν_{in} = 6 $\times 10^5$ Hz, 8 $\times 10^5$ Hz, and 10^6 Hz are considered. Other parameters including dust density and T_e/T_i are varied accordingly to match the experimental observations. Smaller collision frequencies show the best agreement with the data presented in Figure 4. Both solid (n_d/n_{e0} =100%, T_e/T_i =2, ν_{in} =6 $\times 10^5$ Hz) and dashed (n_d/n_{e0} =100%, T_e/T_i =2, ν_{in} =8 $\times 10^5$ Hz) show 40% reduction in signal strength during heating turn-on and 50% enhancement

after the heater turn-off. A slow recovery is observed for both collision frequencies which is in agreement with the data shown in Figure 4. Increasing the ν_{in} to 10^6 Hz enhances the suppression about 0.2 during heating, but the turn-off overshoot stays about the same. The dust density is increased about 5% and T_e/T_i =2.5 is considered. Therefore, measurement of T_e/T_i during heating using an ISR (incoherent scatter radar) can be used as an input to the model which may lead to an good estimation of neutral density. According to Figure 5b, no recovery during heating on is observed for dust particles of 4 nm. The recovery time for dust radii 1 nm and 1.5 nm shown in Figure 5a is negligible and matches the experimental observations. Therefore, the computational results contradict the conclusion by Belova et al., (2006) who proposed the presence of dust particles larger than 10 nm for not observing the recovery during heater on period. The only difference between the computational results in Figure 5 and the observations in Figure 4 is a slower decay time of the turn-off overshoot at higher collision frequencies.

Another parameter that can affect the amplitude of electron density fluctuations during heater turn-on is the recombination of electrons and ions. The recombination time $\tau_{recom} \approx \frac{1}{\gamma n_{i0}} \frac{1}{\sqrt{r_h}}$ where γ is the recombination rate and r_h is the ratio of electron temperature increase during heating. The effect of recombination rate τ_{recom} on the temporal behavior of PMWE during heater turn-on and off is shown in Figure 6. As can be seen, increasing the recombination rate changes the turn-off overshoot and suppression level significantly. The suppression level reduces about 20 percent and the turn-off overshoot is increased from 1.2 to 1.7 when τ_{recom} increased by a factor of 1.7. It should be noted that the effect of recombination rate was overlooked in the previous studies. Therefore, the recovery of the signal during heating could be a result of τ_{recom} variation. The dashed-line curve

with recombination rate 1.5×10^{-12} m^3s^{-1} is in quite reasonable agreement with the experimental observations including suppresion level, turn-off overshoot, fall time and rise time. The rise time of turn-off overshoot is about 2 s and the relaxation time to undisturbed value is about 20 s.

4. HF PMWE

While there have been investigations of PMWE heating experiments in the VHF band, there is no computational modelling or experimental observation of HF PMWE. Considering that the behavior of the temporal evolution of HF PMWE is expected to be different than VHF PMWE as a result of longer irregularity wavelengths, the first computational modeling of HF PMWE is considered in this paper. Figure 7 shows the computational results for temporal evolution of electron irregularities associated with PMWE at 8 MHz and average charge on dust particles. The comparison of the electron fluctuation amplitude (again related to radar cross-section) and the average dust charge Z_d shows that electron density fluctuation amplitude increases during HF pump heating. The average charge on the dust particles is normalized to its value before the heater turn-on. The average charge on dust particles is increased by a factor of 3.5 during heating and returns to undisturbed value after heater turn-off. Small dust radius of 1 nm with density about 130% relative to the background electron density are considered. It is assumed that the irregularity scale size corresponds to a radar frequency of 8 MHz. It is evident that the charge and fluctuation amplitude have very similar behavior and much can be learned about the charging from the radar return. Therefore, enhancement of the irregularity amplitude after heater turn-on in the HF band is a direct manifestation of the dust charging process. Considering the similarity of these two curves, HF PMWE heating may

be used to study fundamental physics of the dust charging process in space. It should be noted that the electron density irregularity amplitude during HF PMSE heating also is very closely related to the temporal evolution of charge on the dust particles (Scales and Mahmoudian, 2016). The main difference between the PMSE and PMWE source regions are the dust radius and density, background electron temperature and density, and plasma/dust-neutral collision frequencies. According to Eq. (12), the diffusion timescale is proportional to ν_{in}. Therefore, τ_{diff} is typically larger in the PMWE source region. This implies the ratio of τ_{diff} to τ_{chg} may typically be larger than that in PMSE. Therefore the conditions for turn-on enhancement of PMWE may possibly be more favorable. It is note-worthy that including photo-detachment current will reduce the average charge on the dust particles and as a result a weaker turn-on overshoot is expected.

Another important parameter that affects the amplitude of turn-on overshoot is the dust radius. Figure 8 shows the time evolution of PMWE at 8 MHz during radiowave heating for dust radius variation from 3 nm to 8 nm. The dust density to background plasma density is 100% to be consistent with previous in-situ measument of MSP in PMWE region (Baumann et al., 2013). The electron temperature is elevated by a factor of 2 during heating. As can be seen, the corresponding radar echoes are expected to be enhanced by a factor of 3.5 and 3 after the heater turn-on for r_d=3 nm and 4 nm, respectively. Increasing dust radius to 5 nm and 6 nm, reduces the maximum turn-on overshoot by about 50% and 70%, respectively. No turn-on overshoot is seen for r_d= 7 nm and 8 nm. Therefore, the smaller meteoric smoke particles in the PMWE source region may increase the chance of HF PMWE enhancement after the heater turn-on.

Figure 9 represents the variation of electron density fluctuation amplitude with varying T_e/T_i at 8 MHz during radiowave heating. As the electron temperature enhancement ratio during heating increases, the maximum amplitude of backscattered radar signal and turn-on overshoot reduces. The turn-on overshoot amplitude reaches 3.8 for $T_e/T_i = 3$ and 2.5 for $T_e/T_i = 7$. While the enhancement of radar signal is observed in the entire heating cycle for $T_e/T_i = 3$, the enhanced signal is observed only for 20 sec after the heater turn-on and drops below one after that for T_e/T_i =7. The enhanced radar signal decays to its initial value within 50 s after the turn-off for $T_e/T_i = 3$ and 4 and eventually reaches the equilibrium state. The recovery time of radar echoes for T_e/T_i= 5, 6 and 7 is about 200 s. According to Eq. (11), increasing the T_e/T_i ratio reduces the charging timescale while the reduction in electron density increases τ_{chg} since the charging time is inversely proportional to n_e. Therefore, there is a competition between the increased charging due to increase in temperature but a decrease due to reduction in electron density. As can be seen in Figure 9, the maximum amplitude of turn-on overshoot reduces by increasing T_e/T_i which is due to the larger reduction in electron density with increasing T_e/T_i. Considering that HF radar is signicantly affected by D-region absorption, measurement with high time resolution is required to observe HF turn-on overshoot during experiment. As the dust density and radius increases, the chance of observing the turn-on overshoot reduces. Based on numerical simulations with $1 < T_e/T_i < 2$, the chance of observing turn-on overshoot at 8 MHz during PMWE heating experiment may be increased. Therefore, considering the parameters used in Figure 9, the range $1 < T_e/T_i < 2$ may be most efficient for observing the turn-on overshoot.

5. Conclusions

Unlike polar mesospheric summer echoes (PMSE), polar mesospheric winter echoes (PMWE) are less studied and understood. The computational study of active modulation of PMWE by high power radiowaves at 8 MHz, 56 MHz, and 224 MHz, has been presented in this study. The available radar frequencies at the EISCAT facility are considered. Variation of dust plasma parameters associated with PMWE such as dust radius, dust density, recombination rate, electron- and dust-neutral collision frequencies, and electron temperature enhancement ratio are included. The important role of photodetachment current and its effects on the agreement of experimental observation with the computational results is investigated. Specifically, two sets of parameters are included in this paper for dust radius. It has been shown for the first time that the dependence of recombination rate on T_e/T_i affects the time evolution of PMWE signal significantly during radiowave heating. Dust radius as small as 1 nm as well as dust radius of 4 nm is used. Computational results derived from different sets of parameters are considered and compared with observations at 224 MHz and 56 MHz. The agreement between the model results and the observations show the high potential of remote sensing of dust and plasma parameters associated with PMWE. Measurement of T_e/T_i using ISR and simultaneous observations in two frequency bands may lead to a more accurate estimation of dust density and radius. Although it has been predicted that including dust particles smaller than 1nm will not qualitatively change the results, it requires a more sophisticated charging model and is the subject of future investigation.

The enhancement of backscattered signal in the HF band during PMWE heating is predicted. The required background dust (MSP)-plasma parameters as well as heater

power (T_e/T_i) for the observation of turn-on overshoot are investigated. It has been shown that the similarity of the temporal evolution of electron density fluctuation (radar echoes) in the HF band and average charge on the dust particles can be used to study the fundamental physics associated with the dust charging in the PMWE source region. Further active experiments of PMWEs should be pursued in the HF band to illuminate the fundamental charging physics in the space environment and get more insight to this unique medium. It has been determined that collision frequency and particle size in PMWE are more important to observing the turn-on overshoot. Considering that there has been no rocket measurement during PMWE in the past due low rate of occurrence, conducting PMWE heating experiments along with the computational modeling in the future could be useful approach to study the role of MSP in PMWE formation.

Acknowledgments. AM was supported through a research grant in the Institute of Geophysics at the University of Tehran. Data used in this paper are availbale upon request.

References

Baumann, C., Rapp, M., Kero, A., and Enell, C.-F.: Meteor smoke influences on the D-region charge balance: Review of recent in situ measurements and one-dimensional model results, Ann. Geophys., 31, 2049-2062, doi:10.5194/angeo-31-2049-2013, 2013.

Belova, E., Smirnova, M., Rietveld, M.T., Isham, B., Kirkwood, S., and Siergienko, T, First observation of the overshoot effect for polar mesospheric winter echoes during radiowave electron temperature modulation, Geophys. Res. Lett, 35, 2008. doi: 10.1029/2007GL032457

Bernstein, I.B. and I.N. Rabinowitz, Theory of electrostatic probes in a low density plasma, Phys. Fluids, 2, 112-121, 1959.

Biebricher, A., and O. Havnes (2012), Non-equilibrium modeling of the PMSE Overshoot Effect revisited: A comprehensive study, J. Plasma Phys., 78, 303319, doi:10.1017/S0022377812000141.

Brasseur, G., and P. C. Simon, Stratospheric chemical and thermal response to long-term variability in solar irradiance, J. Geophys. Res., 86, 7343-7362, 1981.

Chen, C. and W.A. Scales, Electron temperature enhancement effects on plasma irregularities associated with charged dust in the Earths mesosphere, J. Geophys. Res., 110, A12313, doi:10.1029/2005JA011341, 2005.

Chilson, P. B., Belova, E., Rietveld, M. T., Kirkwood, S., and Hoppe, U.: First artificially induced modulation of PMSE using the EISCAT heating facility, Geophys. Res. Lett., 27, 38013804, 2000.

Friedrich, M., M. Rapp, T. Blix, U.-P. Hoppe, K. Torkar, S. Robertson, S. Dickson, and K. Lynch (2012), Electron loss and meteoric dust in the mesosphere, Ann. Geophys., 30, 14951501, doi:10.5194/angeo-30-1495-2012.

Havnes, O., J. Trim, T. Blix, W. Mortensen, L. I. Nsheim, E. Thrane, and T. Tnnesen (1996), First detection of charged dust particles in the Earth's mesosphere, J. Geophys. Res., 101(A5), 1083910847, doi:10.1029/96JA00003.

Havnes, O.: Polar Mesospheric Summer Echoes (PMSE) overshoot effect due to cycling of artificial electron heating, J. Geophys. Res., 109, A02309, doi:10.1029/2003JA010159,2004

Havnes, O., and M. Kassa (2009), On the sizes and observable effects of dust particles in polar mesospheric winter echoes, J. Geophys. Res., 114, D09209, doi:10.1029/2008JD011276.

Havnes, O., C. La Hoz, M. T. Rietveld, M. Kassa, G. Baroni, and A. Biebricher (2011), Dust charging and density conditions deduced from observations of PMWE modulated by artificial electron heating, J. Geophys. Res., 116, D24203, doi:10.1029/2011JD016411.

Havnes, O, Pinedo, H, La Hoz, C, Senior, A, Hartquist, TW, Rietveld, MT and Kosch, MJ (2015), A comparison of overshoot modelling with observations of polar mesospheric summer echoes at radar frequencies of 56 and 224 MHz. Annales Geophysicae, 33 (6). 737 - 747. ISSN 0992-7689.

Hunten, D. M., Turco, R. P., and Toon, O. B.: Smoke and Dust Particles of Meteoric Origin in the Mesosphere and Stratosphere, J. Atmos. Sci., 37, 13421357, 1980.

Inhester, B., J. C. Ulwick, J. Y. N. Cho, M. C. Kelley, and G. Schmidt (1994), Consistency of rocket and radar electron density observations: Implication about the anisotropy of mesospheric turbulence, J. Atmos. Terr. Phys., 52, 855873.

Kavanagh, A.J., Honary, F., Rietveld, M.T., and A. Senior, First observations of the artificial modulation of polar mesosphere winter echoes. Geophys. Res. Lett 33, L19801, 2006. doi:10.1029/2006GL02756.

Kero, A., C.-F. Enell, A. J. Kavanagh, J. Vierinen, I. Virtanen, and E. Turunen (2008), Could negative ion production explain the polar mesosphere winter echo (PMWE) modulation in active HF heating experiments?, Geophys. Res. Lett., 35, L23102, doi:10.1029/2008GL035798.

Kirkwood, S., P. Chilson, E. Belova, P. Dalin, I. Haggstrom, M. Rietveld, and W. Singer (2006a), Infrasound: The cause of strong Polar Mesosphere Winter Echoes?, Ann. Geophys., 24, 475491.

Kirkwood, S., E. Belova, U. Blum, C. Croskey, P. Dalin, K.-H. Fricke, R. A. Goldberg, J. Manninen, J. D. Mitchell, and F. Schmidlin (2006b), Polar Mesosphere Winter Echoes during MaCWAVE, Ann. Geophys., 24, 12451255.

Kirkwood, S., Barabash, V., Belova, E., Nilsson, H., Rao, T. N., Stebel, K., Osepian, A., and Chilson, P. B.: Polar Mesosphere Winter Echoes during Solar Proton Events, Adv. Polar Upper Atmos. Res., 16, 111125, 2002.

Knappmiller et al., S. Knappmiller, M. Rapp, S. Robertson, J. Gumbel (2011), Charging of meteoric smoke and ice particles in the mesosphere including photoemission and photodetachment rates J. Atmos. Sol. Terr. Phys., 73 (2011), pp. 2212–2220.

La Hoz, C., and O. Havnes (2008), Artificial modification of polar mesospheric winter echoes with an RF heater: Do charged dust particles play an active role?, J. Geophys. Res., 113, D19205, doi:10.1029/2008JD010460.

Latteck, R., and I. Strelnikova (2015), Extended observations of polar mesosphere winter echoes over Andya (69N) using MAARSY, J. Geophys. Res. Atmos., 120, 82168226, doi:10.1002/2015JD023291.

Lubken, F.-J., Strelnikov, B., Rapp, M., Singer, W., Latteck, R., Brattli, A., Hoppe, U.-P., and Friedrich, M.: The thermal and dynamical state of the atmosphere during polar mesosphere winter echoes, Atmos. Chem. Phys., 6, 13-24, doi:10.5194/acp-6-13-2006, 2006.

Mahmoudian, A., Scales, W. A., Kosch, M. J., Senior, A., and Rietveld, M.: Dusty space plasma diagnosis using temporal behavior of polar mesospheric summer echoes during active modification, Ann. Geophys., 29, 2169-2179, doi: 10.5194/angeo-29-2169-2011, 2011.

Mahmoudian, A. and W. A. Scales, Temporal evolution of radar echoes associated with mesospheric dust clouds after turn-on of radiowave heating, J. Geophys. Res., doi:10.1029 /2011 JD017166, 2012.

Nishiyama, T., K. Sato, T. Nakamura, M. Tsutsumi, T. Sato, M. Kohma, K. Nishimura, Y. Tomikawa, M. K. Ejiri, and T. T. Tsuda (2015), Height and time characteristics of seasonal and diurnal variations in PMWE based on 1 year observations by the PANSY radar (69.0°S, 39.6°E), Geophys. Res. Lett., 42, 21002108, doi:10.1002/2015GL063349.

Rapp, M., and F. J. Lubken, Modeling of positively charged aerosols in the polar summer mesopause region, Earth Planets Space, 51, 799 807, 1999.

Rapp, M. and F.J. Lubken (2004), Polar mesosphere summer echoes (PMSE): Review of observations and current understanding, Atmos. Chem. Phys., 4, 26012633.

Rapp, M., Charging of mesospheric aerosol particles: the role of photodetachment and photoionization from meteoric smoke and ice particles, Annales Geophys. 27, 24172422, 2009.

Rosenberg, M., J. Vac. Sci. Technol., Ion-dust streaming stabilities in processing plasmas, 14, 631, 1996.

Rosenberg, M., and P. K. Shukla, Dust-acoustic-drift wave instability in a space dusty plasma, J. Geophys. Res., 107(A12), 1492, doi:10.1029/2002JA009539, 2002.

Robertson, et al., (2009), Mass analysis of charged aerosol particles in NLC and PMSE during the ECOMA/MASS campaign, Ann. Geophys., 27, 12131232 (http://www.ann-geophys.net/special$_issue$219.*html*).

Robertson, S., Dicksom, S., Horanyi, M., Sternovsky, Z., Friedrich, M., Janches, D., Megner, L., and Williams, B.: Detection of meteoric smoke particles in the mesosphere by a rocket-borne mass spectrometer, J. Atmos. Sol. Terr. Phys., 118, 161179, 2014

Russell, J. M., et al. (2009), Aeronomy of Ice in the Mesosphere (AIM): Overview and early science results, J. Atmos. Sol. Terr. Phys., 71, 289299.

Scales, W.A. and Mahmoudian, A. (2016), Charged dust phenomena in the near Earth space environment, Reports on Progress in Physics, Vol 79, No 10, http://dx.doi.org/10.1088/0034-4885/79/10/106802.

Senior, A., A. Mahmoudian, H. Pinedo,C. La Hoz, M. T. Rietveld, W. A. Scales,and M. J. Kosch (2014), First mod-ulation of high-frequency polarmesospheric summer echoes byradio heating of the ionosphere,Geophys. Res. Lett., 41, 53475353,doi:10.1002/2014GL060703.

Schmitter, E. D.: Remote sensing planetary waves in the midlatitude mesosphere using low frequency transmitter signals, Ann. Geophys., 29, 1287-1293, doi:10.5194/angeo-29-1287-2011, 2011.

Shukla, P. D., and A. A. Mamun (2002), Introduction to Dusty Plasma Physics, Inst. of Phys., Bristol, U. K.

Strelnikova, I., M. Rapp, S. Raizada, and M. Sulzer (2007), Meteor smoke particle properties derived from Arecibo incoherent scatter radar observations, Geophys. Res. Lett., 34, L15815, doi:10.1029/2007GL030635.

Zeller, O., M. Zecha, J. Bremer, R. Latteck, and W. Singer (2006), Mean characteristics of mesosphere winter echoes at mid and high latitudes, J. Atmos. Sol. Terr. Phys., 68, 1087 1104.

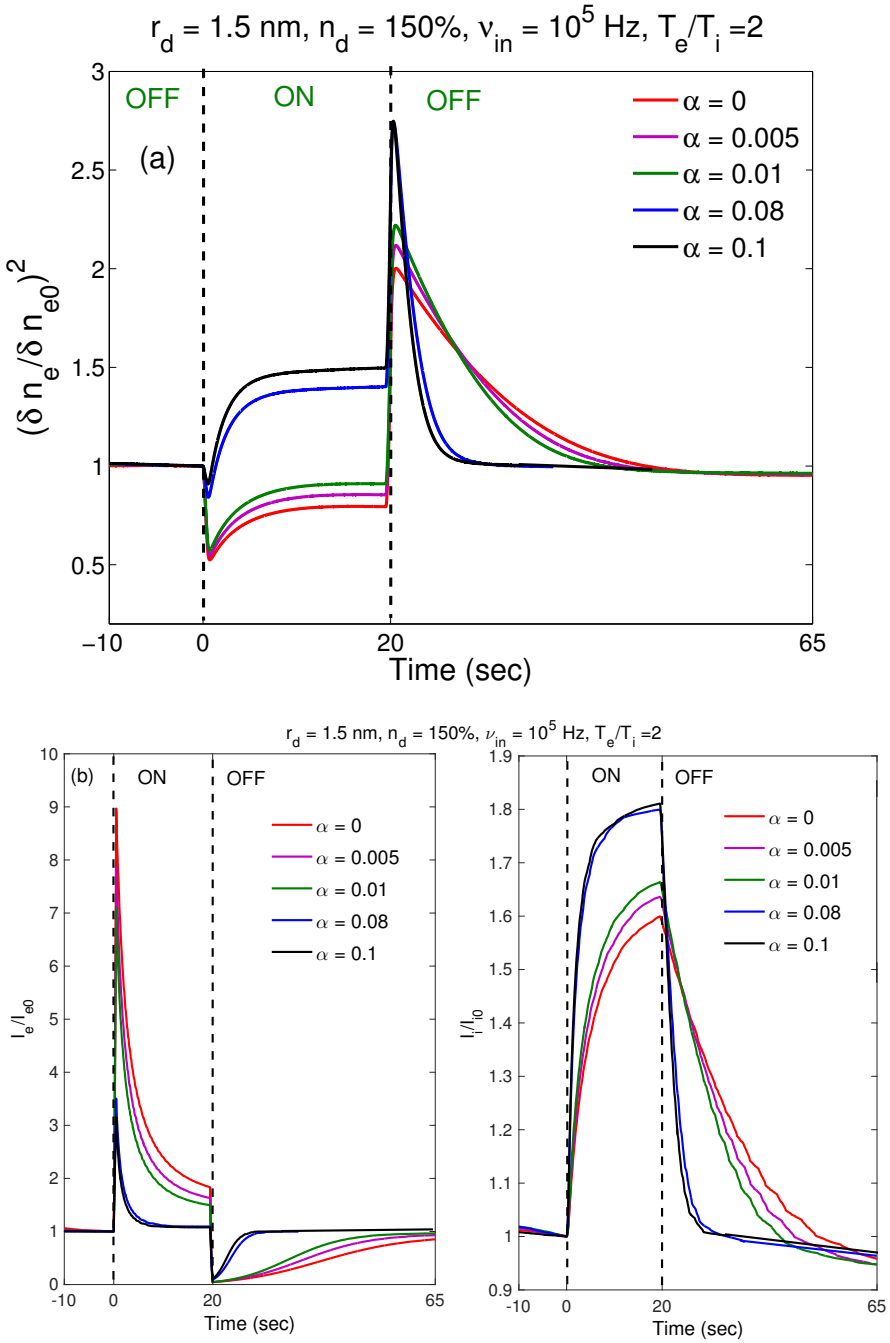

Figure 1. Variation of a) electron irregularity amplitude and b) normalized total electron (on the left) and ion (on the right) currents onto the dust particles associated with temporal evolution of HF PMWE heating at 24 MHz. α denotes photo-detachment current coefficient.

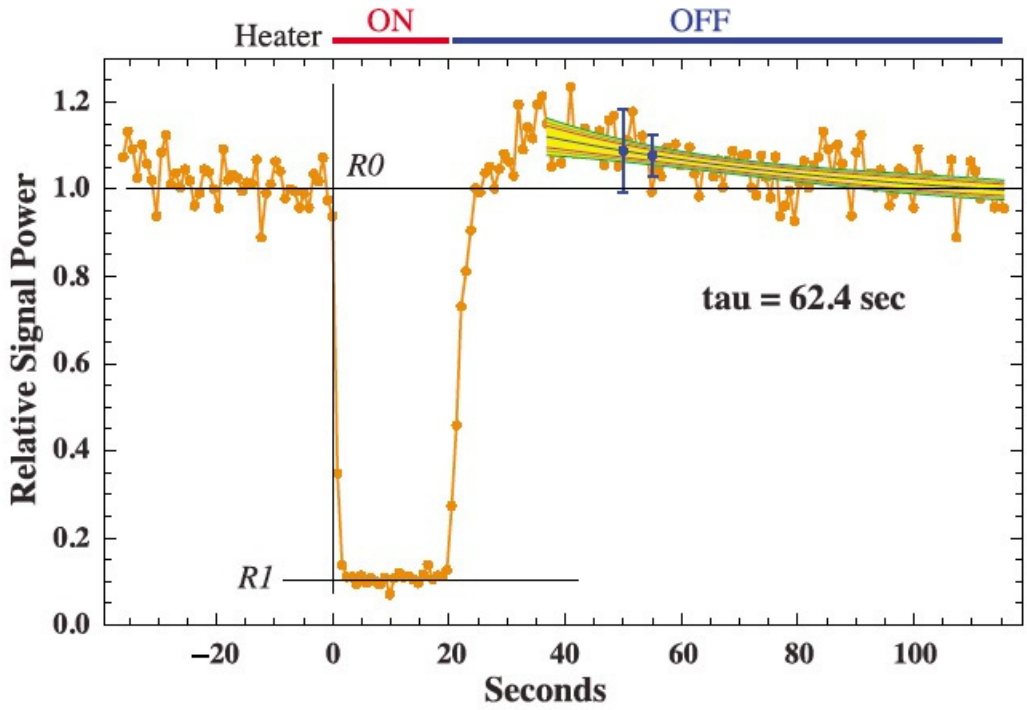

Figure 2. Average curves of modulated PMWE at 56 MHz for 68 heating cycles in the altitude range 58.1 and 63.2 km observed by Havnes et l., (2011). Epoch analysis of two periods of 20-second on heating. The heater was turned-on at t = 0 s.

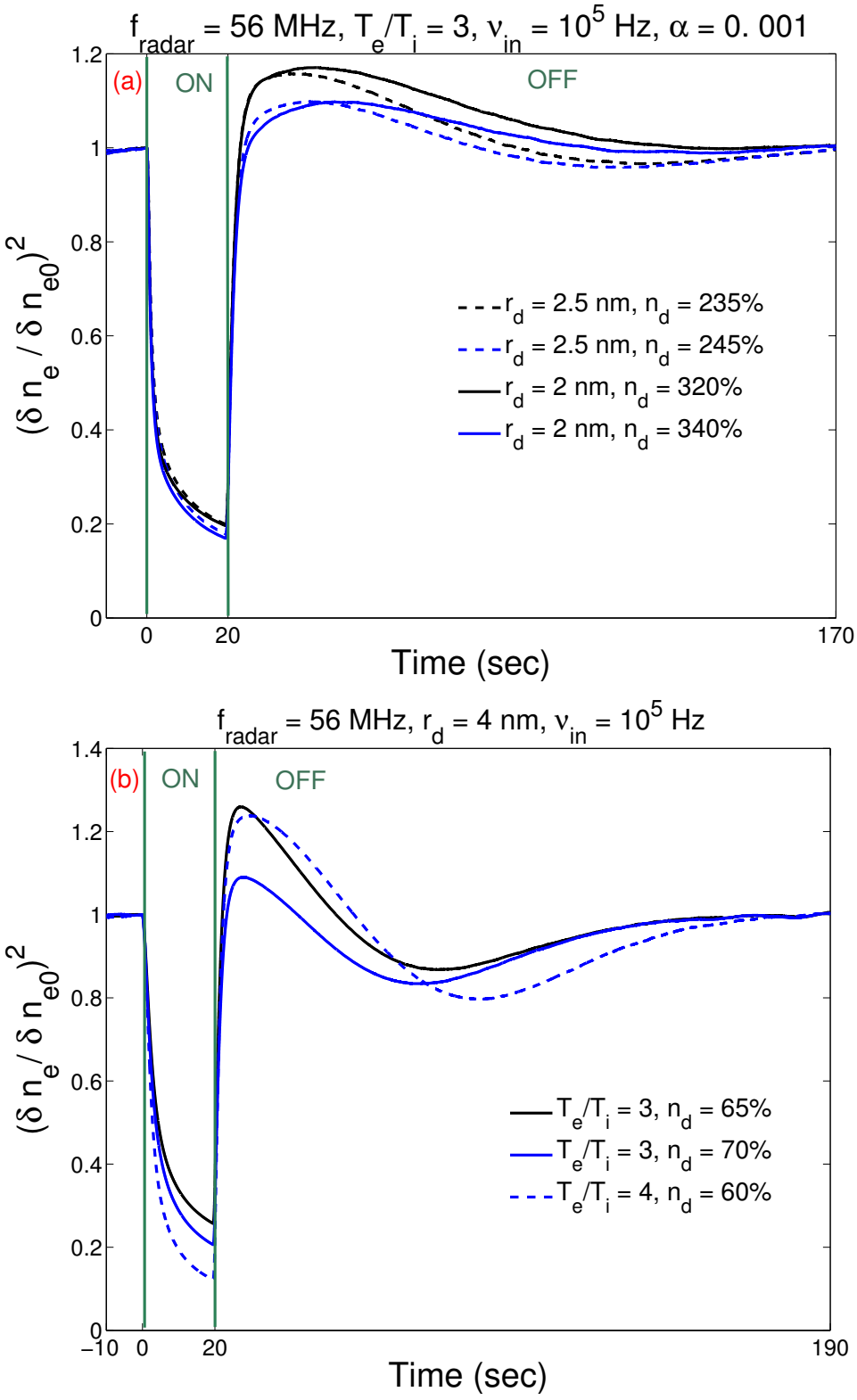

Figure 3. Temporal behavior of PMWE during radiowave heating at 56 MHz for a) r_d =2 nm and 2.5 nm, and b) $r_d = 4$ nm. The heater is turned-on at t = 0 s and turned-off at t = 20 s.

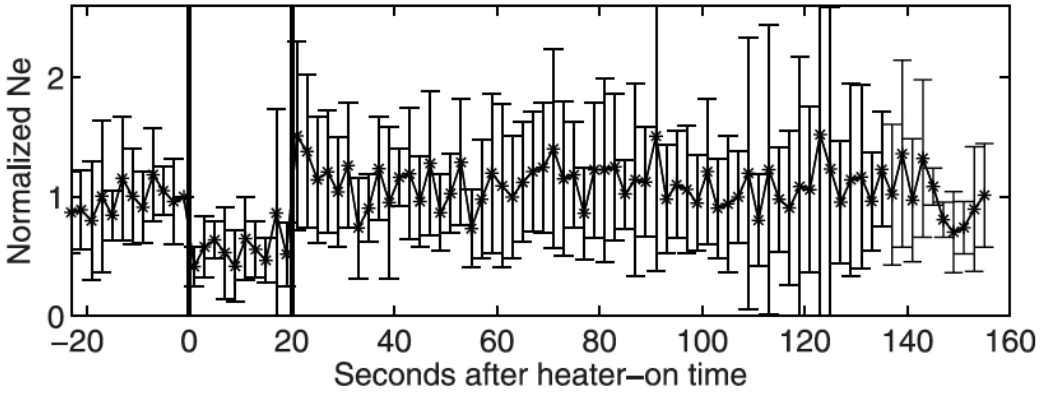

Figure 4. Epoch analysis of PMWE layer during 7 heating cycles. Data were normalized by the values observed 12 s prior to the time of heating switching on. The heater is turned-on at t = 0 s and was on for 20 s. The figure is reproduced after Belova et al., (2008).

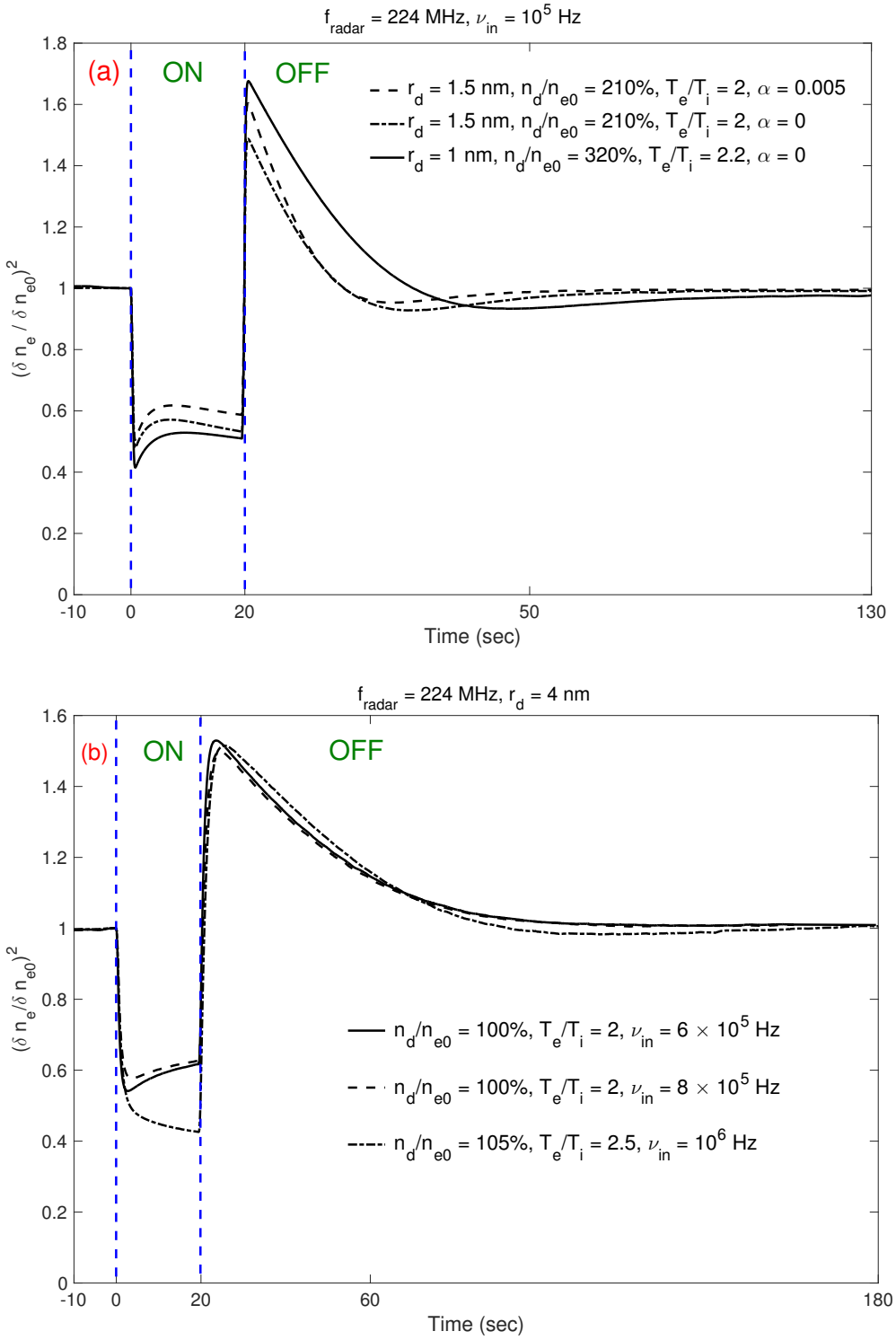

Figure 5. Temporal evolution of PMWE during radiowave heating at 224 MHz for a) $r_d = 1$ nm and 1.5 nm and b) $r_d = 4$ nm with varying ion-, dust-, and electron-neutral collision frequencies. The heater is turned-on at t = 0 s and turned-off at t = 20 s.

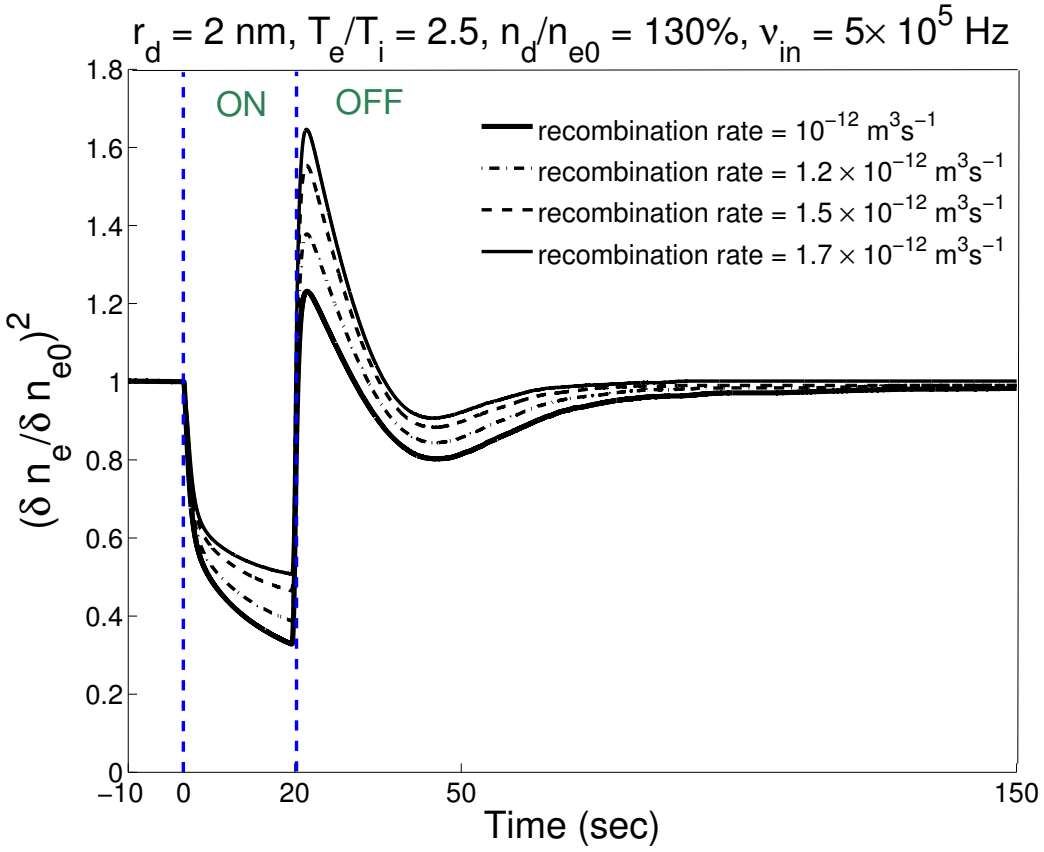

Figure 6. Temporal evolution of PMWE during radiowave heating at 224 MHz with varying recombination rate. The heater is turned-on at t = 0 s and turned-off at t = 20 s.

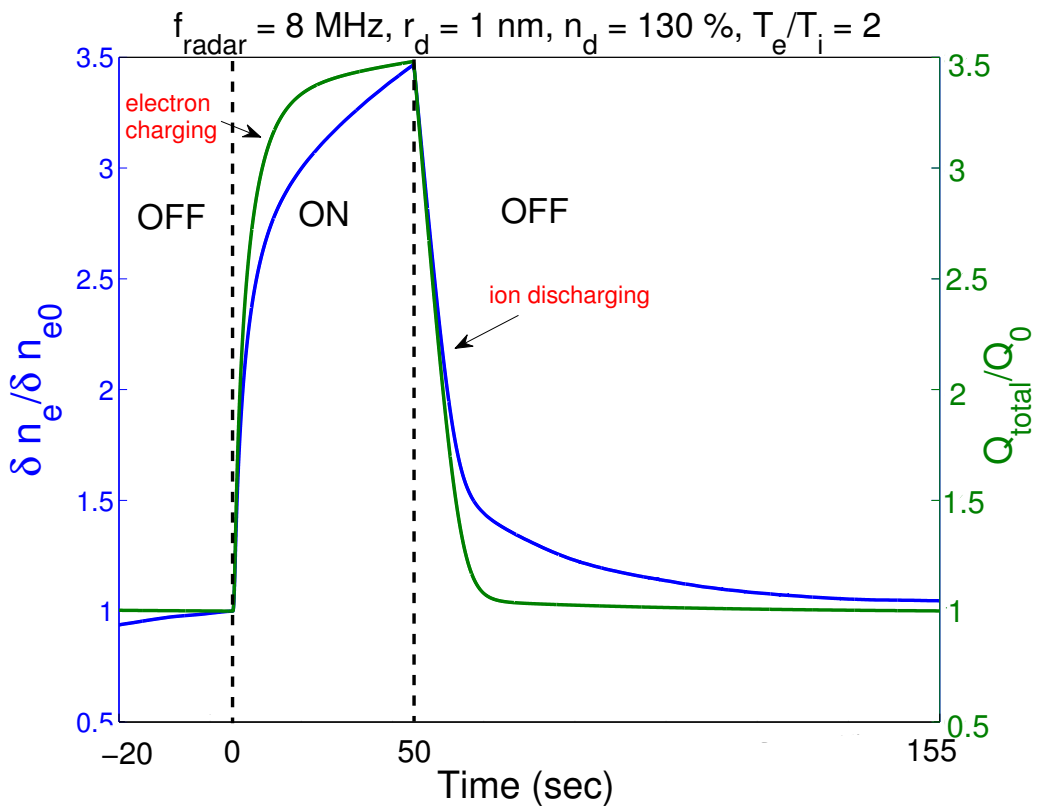

Figure 7. Comparison of average dust charge and electron fluctuation associated with HF radar scatter for PMWE heating indicating similar temporal behavior.

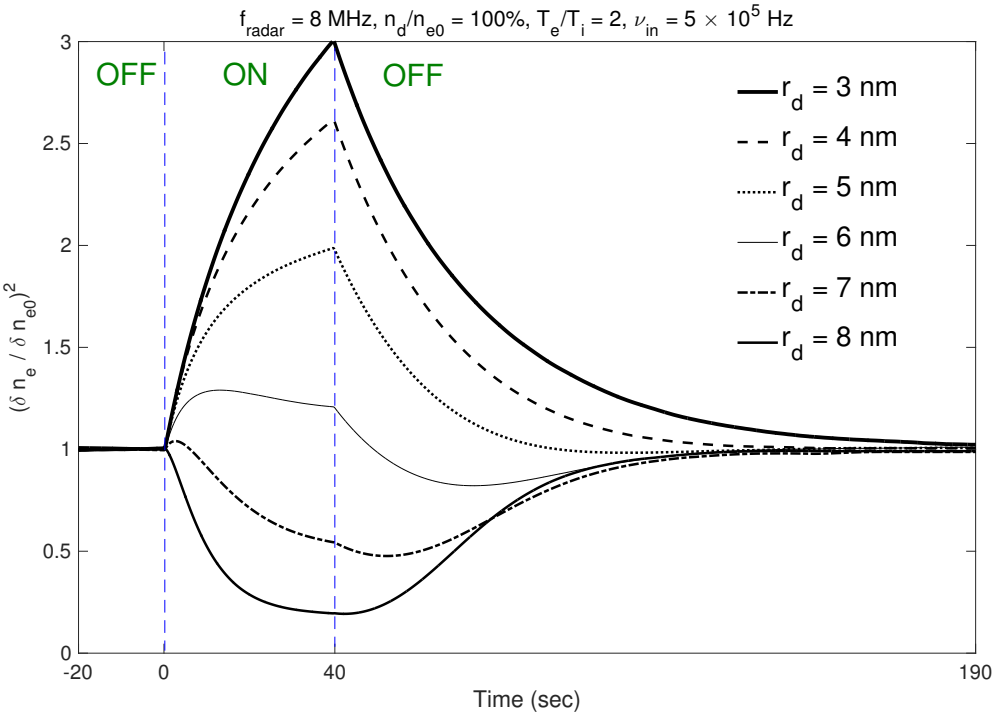

Figure 8. Time evolution of electron density fluctuation amplitude in PMWE region during radiowave heating with varying dust radius. The heater is turned at t = 0 s and is on for 40 s.

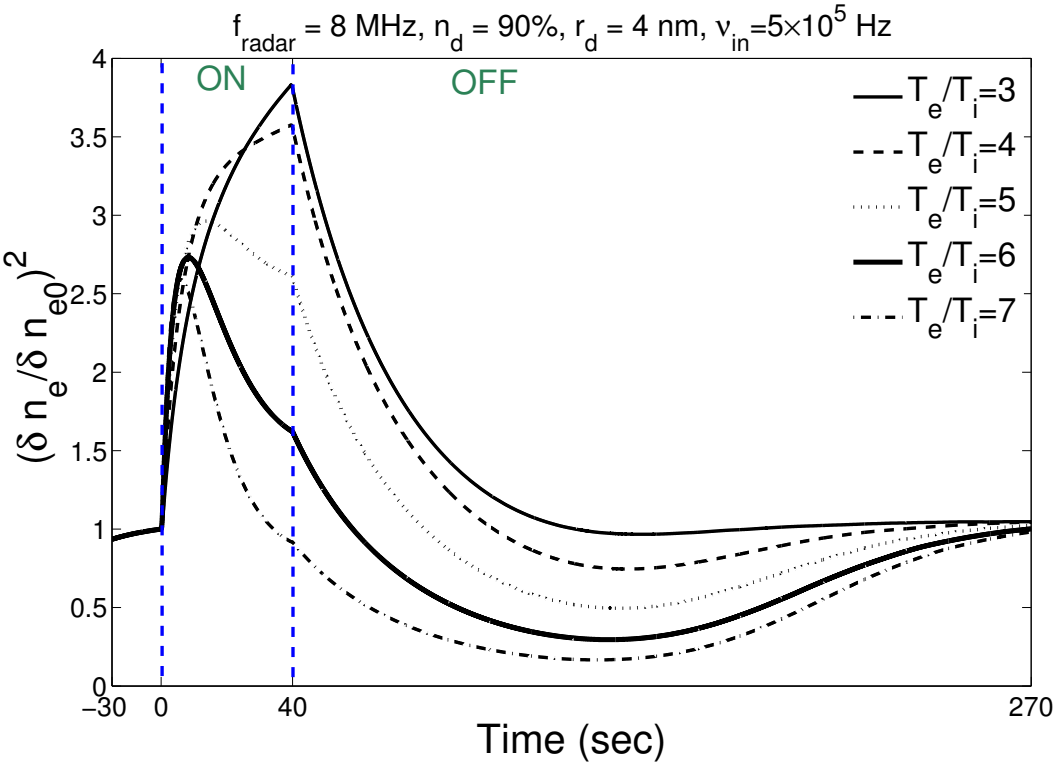

Figure 9. Time evolution of electron density fluctuation amplitude in PMWE region during radiowave heating with varying dust radius. The heater is turned at t = 0 s and is on for 40 s.